EPJ Web of Conferences **75**, 06012 (2014)
DOI: 10.1051/epjconf/20147506012

$Fe_{50}Pt_{50-x}Pd_x$ alloy thin films with $L1_0$ structure epitaxially grown on MgO(001) substrates

Akira Itabashi[1], Mitsuru Ohtake[1], Fumiyoshi Kirino[2], and Masaaki Futamoto[1,a]

[1]Faculty of Science and Engineering, Chuo University, 1-13-27 Kasuga, Bunkyo-ku, Tokyo 112-8551, Japan
[2]Graduate School of Fine Arts, Tokyo University of the Arts, 12-8 Ueno-koen, Taito-ku, Tokyo 110-8714, Japan

Abstract. $Fe_{50}Pt_{50-x}Pd_x$ (at. %, x = 0, 12.5, 25, 37.5, 50) alloy epitaxial films are prepared on MgO(001) substrates at temperatures ranging from room temperature to 600 °C by radio-frequency magnetron sputtering. The effects of substrate temperature and Pd/Pt composition on the order degree, c-axis distribution, and magnetic property are investigated. With increasing the substrate temperature, $L1_0$ ordering is enhanced for all the compositions. The order degree of film deposited at 600 °C decreases from 0.37 to 0.23 as the x value increases from 0 to 12.5 at. %. With further increasing the x value, the order degree increases up to 0.69. The $Fe_{50}Pt_{50-x}Pd_x$ films with $x \geq 25$ consist of only an $L1_0$(001) single-crystal with the c-axis perpendicular to the substrate surface, whereas the films with $x < 25$ involve two types of $L1_0$(100) variant with the c-axis lying in the film plane in addition to $L1_0$(001) variant. The c-axis distribution is influenced by the Pd/Pt composition. The magnetic anisotropy is reflecting the c-axis distribution and the order degree.

1 Introduction

Ferromagnetic $L1_0$ ordered alloy thin films with the uniaxial magnetocrystalline anisotropy energy (K_u) greater than 10^7 erg/cm^3 and with the easy magnetization axis perpendicular to the substrate surface have been investigated for applications like recording media, magnetoresistive random access memory devices, etc. FePt and FePd alloys around the equiatomic composition have $L1_0$ ordered phase. FePt and FePd bulk crystal with $L1_0$ structure show K_u greater then 10^7 erg/cm^3 along the c-axis [1, 2]. Control of c-axis orientation is an important issue for practical applications as well as achieving a high order degree (S). When a film with $L1_0$ structure is formed on a polycrystalline underlayer consisting of (001)-oriented grains or a single-crystal (001) substrate, there is a possibility that the film involves $L1_0$(100) crystal with the c-axis lying in the film plane in addition to $L1_0$(001) crystal with the c-axis normal to the film surface. In order to investigate the $L1_0$ crystal distribution, well-defined epitaxial films are useful, since the crystallographic orientation can be controlled by single-crystal substrate. FePt [3–5] and FePd [5–7] epitaxial films have been prepared on (001) single-crystal substrates. However, $L1_0$ ordering has been mainly estimated by $2\theta/\omega$-scan out-of-plane X-ray diffraction (XRD). $2\theta\chi/\phi$-scan in-plane XRD needs to be combined to investigate the presence of $L1_0$(100) crystals [5, 8, 9].

In our previous study [5], FePt and FePd films were deposited on MgO(001) substrates at 600 °C. The FePd film consisted of only $L1_0$(001) crystal, whereas the FePt film included $L1_0$(100) crystal in addition to $L1_0$(001) crystal. The S of FePd film (0.69) was higher than that of FePt film (0.37). However, the K_u of fully $L1_0$ ordered FePt alloy (6.6×10^7 erg/cm^3 [1]) is reported to be higher than that of FePd alloy (1.7×10^7 erg/cm^3 [2]). In order to control the c-axis to be perpendicular while enhancing the $L1_0$ ordering, a replacement of Pt site in FePt film with Pd seems useful. Fe(Pt,Pd) films have been prepared on Si substrates with natural oxide layers [10, 11] and MgO(001) single-crystal substrates [12, 13]. However, there are few reports on the structural analysis by taking into account the c-axis distribution. In the present study, $Fe_{50}Pt_{50-x}Pd_x$ (at. %) films are deposited on MgO(001) substrates by varying the Pd content of x from 0 to 50 at. %. The effects of substrate temperature and Pd/Pt composition on the order degree, c-axis distribution, and magnetic property are investigated.

2 Experimental procedure

$Fe_{50}Pt_{50-x}Pd_x$ (x = 0, 12.5, 25, 37.5, 50) alloy films of 40 nm thickness were deposited on MgO(001) substrates at temperatures ranging from room temperature (RT) to 600 °C by using a radio-frequency (RF) magnetron sputtering system equipped with a reflection high-energy electron diffraction (RHEED) facility. The base pressures were lower than 4×10^{-7} Pa. Before film formation, substrates were heated at 600 °C for 1 h in the chamber to obtain clean surfaces. The Ar gas pressure was kept constant at 0.67 Pa. The distance between target and substrate was fixed at 150 mm. $Fe_{50}Pt_{50}$, $Fe_{50}Pt_{37.5}Pd_{12.5}$, $Fe_{50}Pt_{25}Pd_{25}$, $Fe_{50}Pt_{12.5}Pd_{37.5}$, and $Fe_{50}Pd_{50}$ alloy targets of

[a] Corresponding author: futamoto@elect.chuo-u.ac.jp

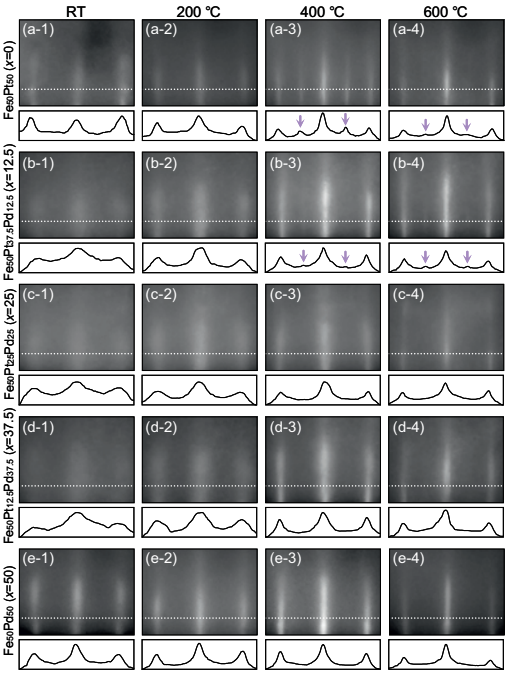

Fig. 1. RHEED patterns and the intensity profiles of (a) $Fe_{50}Pt_{50}$, (b) $Fe_{50}Pt_{37.5}Pd_{12.5}$, (c) $Fe_{50}Pt_{25}Pd_{25}$, (d) $Fe_{50}Pt_{12.5}Pd_{37.5}$, and (e) $Fe_{50}Pd_{50}$ films deposited at (a-1)–(e-1) RT, (a-2)–(e-2) 200 °C, (a-3)–(e-3) 400 °C, and (a-4)–(e-4) 600 °C. The incident electron beam is parallel to MgO[100].

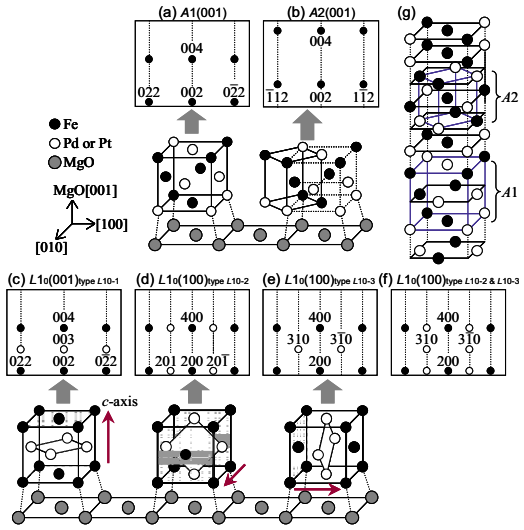

Fig. 2. Schematic diagrams of RHEED patterns simulated for (a) $A1(001)$, (b) $A2(001)$, (c) $L1_0(001)$, (d, e) $L1_0(100)$ single-crystal surfaces. The incident electron beam is parallel to (a, c) [100], (b) [110], (d) [010], or (e) [001]. Schematic diagram of (f) is drawn by overlapping (d) and (e). The filled and open circles respectively correspond to the fundamental and superlattice reflections. (g) Schematic diagram of a crystallographic lattice mixed with $A1$ and $A2$ structures.

3 in diameter were employed and the RF powers for the respective targets were adjusted to be 43, 38, 35, 34, and 35 W, where the deposition rate was 0.02 nm/s for all the materials. The film compositions were confirmed by energy dispersive X-ray spectroscopy and the errors were less than 4 at. % from the target compositions. The surface structure was studied by RHEED. The resulting structure was investigated by $2\theta/\omega$-scan out-of-plane and $2\theta\chi/\phi$-scan in-plane XRDs with Cu-Kα radiation (λ = 0.15418 nm). The magnetization curves were measured by using a vibrating sample magnetometer.

The notations of crystallographic plane and direction are different between disordered $A1$ and ordered $L1_0$ structures. In the present study, however, $A1$-based notation is applied to the $L1_0$ structure for simple comparison with the $A1$ structure.

3 Results and discussion

Figures 1(a-1)–(a-4) show the RHEED patterns and the intensity profiles of $Fe_{50}Pt_{50}$ films deposited at different temperatures. Clear diffraction patterns consisting of streaks are observed for all the films. $Fe_{50}Pt_{50}$ films grow epitaxially on the substrates. The RHEED patterns observed for the films deposited below 200 °C [figures 1(a, b)] correspond to an $A1(001)$ or an $L1_0(001)$ single-crystal surface, as shown by the schematic diagrams of figures 2(a) and (c). The identification is difficult when a streak pattern is observed, since the diffraction patterns are very similar. The crystal structure is thus determined by XRD analysis, which is described later. The RHEED patterns observed for the films deposited above 400 °C apparently involve diffraction patterns from two types of $L1_0(100)$ variant [figures 2(b, c)], as shown by the arrows in the intensity profiles of figures 1(a-3) and 1(a-4). The epitaxial orientation relationships are estimated by RHEED as $A1(100)[100]$, $L1_0(100)[100]_{type\ L10\text{-}1}$, $L1_0(100)[010]_{type\ L10\text{-}2}$, $L1_0(100)[001]_{type\ L10\text{-}3}$ || MgO(001)[100]. The $A1(001)$ and the $L1_0(001)$ crystals are single-crystals, whereas the $L1_0(100)$ crystal consists of two variants whose c-axes are lying in the film plane and rotated around the film normal by 90° each other. Figures 3(a-1)–(a-4) and 4(a-1)–(a-4) show the out-of-plane and in-plane XRD patterns of $Fe_{50}Pt_{50}$ films. Here, the scattering vector of in-plane XRD is parallel to MgO[100]. Only the out-of-plane (002) and in-plane (200) fundamental reflections are observed for the films deposited below 200 °C [figures 3(a-1, a-2), 4(a-1, a-2)]. The crystal structure is thus $A1$. In the in-plane patterns observed for the films deposited above 400 °C [figures 4(a-3, a-4)], (001) superlattice reflections from the $L1_0$-3 type (100) variant whose c-axis is parallel to MgO[100] are recognized. (001) superlattice reflections are also observed in the out-of-plane patterns [figures 3(a-3, a-4)]. These results show that the films deposited above 400 °C consist of a mixture of $L1_0(001)$ and $L1_0(100)$ crystals.

Figures 1(b-1)–(d-1) and (b-2)–(d-2) show the RHEED patterns observed for $Fe_{50}Pt_{50-x}Pd_x$ (x = 12.5, 25, 37.5) ternary alloy films deposited below 200 °C. Diffraction patterns consisting of streaks are observed. Epitaxial $Fe_{50}Pt_{50-x}Pd_x$ films are obtained. The streaks are broader when compared with those observed for the $Fe_{50}Pt_{50}$ films [figures 2(a-1, a-2)]. The result indicates a possibility that another diffraction pattern is overlapped with the diffraction pattern from $A1(001)$ or $L1_0(001)$ crystal. Figures 3(b-1)–(d-1) and (b-2)–(d-2) show the out-of-plane XRD patterns. $A2(002)$ reflections ($A2$: bcc) are recognized around 2θ = 60° in addition to $A1(002)$ reflections. Figures 4(b-1)–(d-1) and (b-2)–(d-2) show the in-plane patterns. $A2(220)$ and $A1(200)$ reflections are overlapped around $2\theta\chi$ = 47°. These results show that $A2(001)$ crystals are involved in the films, as shown in figure 1(g). The crystallographic orientation relationship of $A2(001)$ with respect to the substrate is determined by

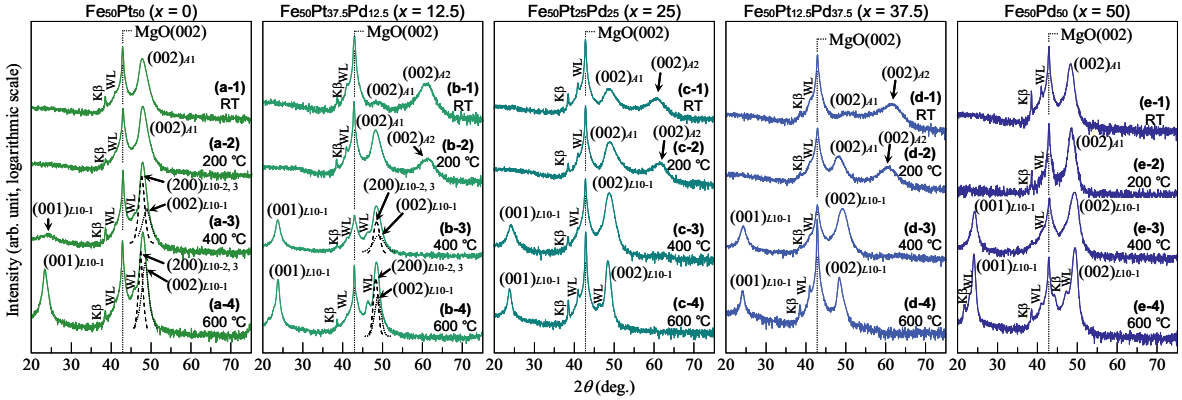

Fig. 3. Out-of-plane XRD patterns of (a) $Fe_{50}Pt_{50}$, (b) $Fe_{50}Pt_{37.5}Pd_{12.5}$, (c) $Fe_{50}Pt_{25}Pd_{25}$, (d) $Fe_{50}Pt_{12.5}Pd_{37.5}$, and (e) $Fe_{50}Pd_{50}$ films deposited on MgO(001) substrates at (a-1)–(e-1) RT, (a-2)–(e-2) 200 °C, (a-3)–(e-3) 400 °C, and (a-4)–(e-4) 600 °C, respectively. The small reflections noted as Kβ and WL are due to Cu-Kβ and W-Lα radiations included in the X-ray source, respectively.

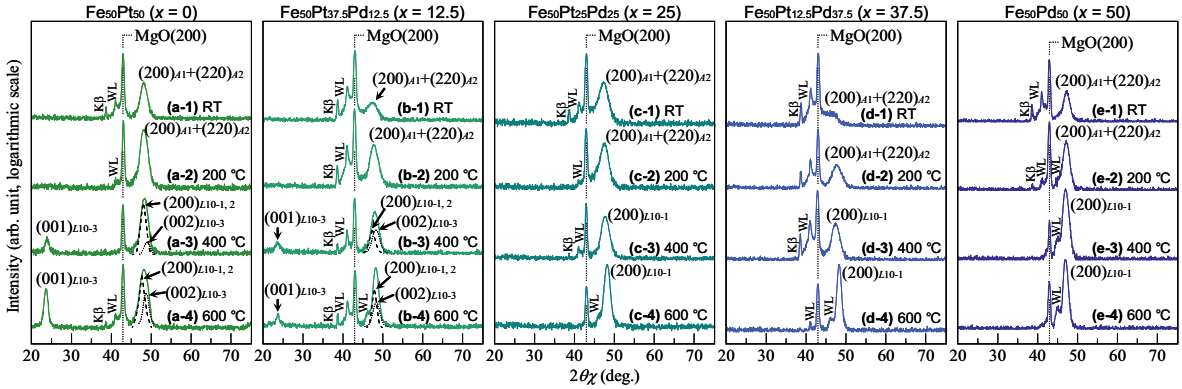

Fig. 4. In-plane XRD patterns of (a) $Fe_{50}Pt_{50}$, (b) $Fe_{50}Pt_{37.5}Pd_{12.5}$, (c) $Fe_{50}Pt_{25}Pd_{25}$, (d) $Fe_{50}Pt_{12.5}Pd_{37.5}$, and (e) $Fe_{50}Pt_{50}$ films deposited on MgO(001) substrates at (a-1)–(e-1) RT, (a-2)–(e-2) 200 °C, (a-3)–(e-3) 400 °C, and (a-4)–(e-4) 600 °C, respectively. The scattering vector is parallel to MgO[100]. The small reflections noted as Kβ and WL are due to Cu-Kβ and W-Lα radiations included in the X-ray source, respectively.

XRDs as $A2(001)[100]$ ‖ MgO(001)[100]. Figure 1(b) shows the schematic diagram of RHEED pattern simulated for an $A2(001)$ surface. The diffraction pattern from $A2(001)$ crystal is very similar to that from $A1(001)$ crystal [figure 1(a)]. Therefore, patterns from $A1$ and $A2$ crystals are considered to be overlapped in the RHEED patterns observed for the $Fe_{50}Pt_{50-x}Pd_x$ films deposited below 200 °C.

Figures 1(b-3)–(d-3) and (b-4)–(d-4) show the RHEED patterns observed for $Fe_{50}Pt_{50-x}Pd_x$ (x = 12.5, 25, 37.5) films deposited at 400 and 600 °C. With increasing the substrate temperature up to 400 °C, sharp streaks are observed. The RHEED patterns observed for the $Fe_{50}Pt_{37.5}Pd_{12.5}$ films involve diffraction patterns from two $L1_0(100)$ variants. On the contrary, formation of $L1_0(100)$ variants is not recognized for the $Fe_{50}Pt_{25}Pd_{25}$ and the $Fe_{50}Pt_{12.5}Pd_{37.5}$ films. Figures 3(b-3)–(d-3), (b-4)–(d-4), 4(b-3)–(d-3), and (b-4)–(d-4) show the XRD patterns. (001) out-of-plane and in-plane reflections are observed for the $Fe_{50}Pt_{37.5}Pd_{12.5}$ films, whereas only (001) out-of-plane reflections are recognized for the $Fe_{50}Pt_{25}Pd_{25}$ and the $Fe_{50}Pt_{12.5}Pd_{37.5}$ films. The $Fe_{50}Pt_{37.5}Pd_{12.5}$ films consist of a mixture of $L1_0(001)$ and $L1_0(100)$ crystals, while the $Fe_{50}Pt_{25}Pd_{25}$ and the $Fe_{50}Pt_{12.5}Pd_{37.5}$ films are $L1_0(001)$ single-crystals. The c-axis is apparently controlled to be perpendicular to the substrate surface by employing a Pd content of x higher than 25 at. %.

Figure 1(e) shows the RHEED patterns observed for $Fe_{50}Pd_{50}$ films. Figures 3(e) and 4(e) show the XRD patterns. When the substrate temperature exceeds 400 °C, (001) out-of-plane reflections appear. Therefore, the crystal structure of films deposited below 200 °C is $A1$ structure, whereas the films deposited above 400 °C are $L1_0(001)$ single-crystals.

The volume percentage ratios of $L1_0(001)$ and $L1_0(100)$ crystals, $V_{(001)}$ and $V_{(100)}$, are calculated from the XRD data by using the following equations,

$$V_{(001)} = \{I_{(002)op}/(I_{(002)op}+I_{(200)op})\}\times 100, \quad (1)$$

$$V_{(100)} = \{I_{(200)op}/(I_{(002)op}+I_{(200)op})\}\times 100. \quad (2)$$

where I is the integrated intensity and the subscripts of (002)op and (200)op respectively correspond to (002) and (200) out-of-plane reflections. The calculation method is reported in our previous papers [9, 14]. Figures 5(a) and (b) show the dependences of Pd content (x) on the $V_{(001)}$ and $V_{(100)}$ values of $Fe_{50}Pt_{50-x}Pd_x$ films deposited at 400 and 600 °C, respectively. The $V_{(001)}$:$V_{(100)}$ ratios of $Fe_{50}Pt_{50}$ (x = 0) films deposited at 400 and 600 °C are 42:58 and 45:55, respectively. With increasing the x value up to 25 at. %, the ratio becomes 100:0 for both cases. The result indicates that the $L1_0$ crystal distribution is not influenced by the substrate temperature but by the Pd/Pt composition.

The order degrees of $L1_0(001)$ crystal ($S_{(001)}$), $L1_0(100)$ crystal ($S_{(100)}$), and film total (S_{total}) are estimated by employing the following equations,

$$S_{(001)} = (I_{(001)op}/I_{(002)op})\times\{(LA)_{(002)op}/(LA)_{(001)op}\} \times[\{(50-x)f_{Pt}+xf_{Pd}+50f_{Fe}\}_{(002)op}/\{(50-x)f_{Pt}+xf_{Pd}+50f_{Fe}\}_{(001)op}]^{1/2}, \quad (3)$$

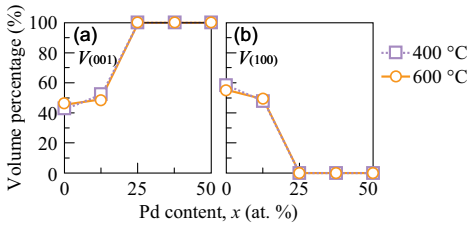

Fig. 5. Volume percentages of (a) $V_{(001)}$ and (b) $V_{(100)}$ of $Fe_{50}Pt_{50-x}Pd_x$ films.

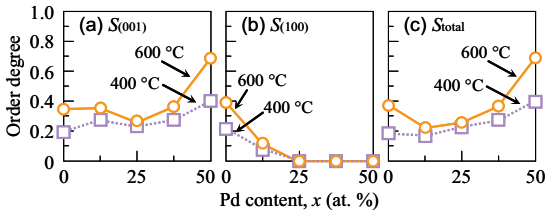

Fig. 6. Order degrees of (a) $S_{(001)}$, (b) $S_{(100)}$, and (c) S_{total} of $Fe_{50}Pt_{50-x}Pd_x$ films.

$$S_{(001)} = (I_{(001)ip}/I_{(002)ip})\times\{(LA)_{(002)ip}/(LA)_{(001)ip}\} \times[\{(50-x)f_{Pt}+xf_{Pd}+50f_{Fe}\}_{(002)ip}/\{(50-x)f_{Pt}+xf_{Pd}+50f_{Fe}\}_{(001)ip}]^{1/2}, \quad (4)$$

$$S_{total} = S_{(001)}(V_{(001)}/100)+S_{(100)}(V_{(100)}/100), \quad (5)$$

where L, A, and f are respectively Lorentz-polarization, absorption, and atomic scattering factors. The details of estimation method is shown in our previous papers [9, 14]. Figure 6 shows the $S_{(001)}$, $S_{(100)}$, and S_{total} values of $Fe_{50}Pt_{50-x}Pd_x$ films deposited at 400 and 600 °C. For all the x values, the films deposited at 600 °C show higher $S_{(001)}$, $S_{(100)}$, and S_{total} values than those deposited at 400 °C. With increasing the x value from 0 to 12.5 at. %, the S_{total} of films deposited at 400 and 600 °C decreases from 0.18 to 0.16 and from 0.37 to 0.23, respectively. As the x value further increases, the S_{total} of films deposited at 400 and 600 °C increases up to 0.40 and 0.69, respectively. The degree of $L1_0$ ordering is promoted for Pd-rich compositions.

Figures 7(a) and (b) show the magnetization curves measured for $Fe_{50}Pt_{50}$ and $Fe_{50}Pd_{50}$ films at different temperatures, respectively. With increasing the substrate temperature, stronger perpendicular magnetic anisotropy is observed for the $Fe_{50}Pd_{50}$ films [figure 7(b)]. The result is due to that $Fe_{50}Pd_{50}$ films consist of only $A1(001)$ or $L1_0(001)$ crystal and that the S_{total} increases with increasing the temperature. Although the $Fe_{50}Pd_{50}$ film with S_{total} = 0.40 (formed at 400 °C) shows perpendicular anisotropy, the $Fe_{50}Pt_{50}$ film with S_{total} = 0.37 (formed at 600 °C) show in-plane anisotropy. The reason is due to that the $Fe_{50}Pt_{50}$ film consist of a mixture of $L1_0(001)$ and $L1_0(100)$ crystals. The magnetic property is apparently influenced by the order degree and the c-axis distribution.

4 Conclusion

$Fe_{50}Pt_{50-x}Pd_x$ alloy films are prepared on MgO(001) substrates. The effects of substrate temperature and Pd/Pt composition on the film structural and magnetic properties are investigated. $L1_0$ ordering is enhanced by increasing the substrate temperature for all the composition. The S_{total} values of $Fe_{50}Pt_{50-x}Pd_x$ films with x values of 0, 12.5, 25, 37.5, and 50 at. % deposited at

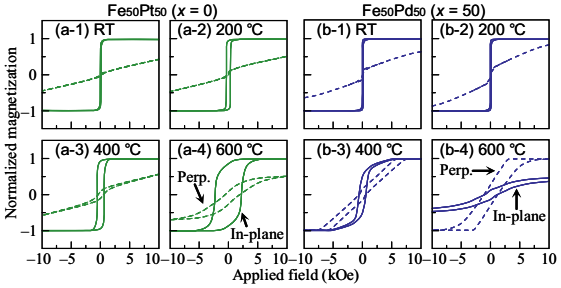

Fig. 7. Magnetization curves measured for (a) $Fe_{50}Pt_{50}$ and (b) $Fe_{50}Pd_{50}$ films deposited on MgO(001) substrates at (a-1)–(b-1) RT, (a-2)–(b-2) 200 °C, (a-3)–(b-3) 400 °C, and (a-4)–(b-4) 600 °C.

600 °C are 0.37, 0.23, 0.25, 0.36, and 0.69, respectively. $L1_0$ ordering is promoted for Pd-rich compositions. The films with $x \geq 25$ are $L1_0(001)$ single-crystals, whereas those with $x < 25$ involve two types of $L1_0(100)$ variant in addition to $L1_0(001)$ variant. The c-axis distribution is influenced by the Pd/Pt composition. The magnetic property is influenced by the order degree and the c-axis distribution.

Acknowledgements

This work was supported by JSPS KAKENHI Grant Number 25420294, JST A-STEP Grant Number AS242Z00169M, and Chuo University Grant for Special Research.

References

1. O. A. Ivanov, L. V. Solina, V. A. Demshina, L. M. Magat, Fiz. Metal. Metalloved. **35**, 81, (1973)
2. A. Ye, Yermakov, V. V. Maykov, Phys. Met. Metall. **69**, 198, (1990)
3. B. M. Lairson, M. R. Visokay, R. Sinclair, B. M. Clemens, Appl. Phys. Lett. **62**, 639 (1993)
4. A. Cebollada, D. Weller, J. Sticht, G. R. Harp, R. F. C. Farrow, R. F. Marks, R. Savoy, J. C. Scott, Phys. Rev. B **50**, 3419 (1994)
5. M. Ohtake, S. Ouchi, F. Kirino, M. Futamoto, J. Appl. Phys. **111**, 07A708 (2012)
6. V. Gehanno, A. Marty, B. Gilles, Y. Samson, Phys. Rev. B **55**, 12552 (1997)
7. P. R. Aitchison, J. N. Chapman, V. Gehanno, I. S. Weir, M. R. Scheinfein, S. McVitie, A. Marty, J. Magn. Magn. Mater. **223**, 138 (2001)
8. S. Jeong, T. Ohkubo, A. G. Roy, D. E. Laughlm, M. E. McHenry, J. Appl. Phys. **91**, 6863 (2002)
9. Y. Numata, A. Itabashi, M. Ohtake, F. Kirino, M. Futamoto, IEEE Trans. Magn. **50**, 2101304 (2014)
10. S. Jeong, A. G. Roy, D. E. Lauglin, M. E. McHenry, J. Appl. Phys. **91**, 8813 (2002)
11. S. Jian, G. Chen, J. S. Jang, Y. Liao, Thin Solid Films, **517**, 4883 (2009)
12. S. Yoshimura, S. Omiya, G. Egawa, H. Saito, J. Bai, J. Phys. Conf. Ser. **266**, 012114 (2011)
13. P. He, L. Ma, Z. Shi, G. Y. Guo, J. -G. Zheng, Y. Xin, S. M. Zhou, Phys. Rev. Lett. **109**, 066402 (2012)
14. M. Ohtake, M. Futamoto, IEEE Trans. Magn. **50**, 2100204 (2014)